Magnetic ordering in $TbMn_{0.5}Cr_{0.5}O_3$ studied by neutron diffraction and first-principles calculations

M. Staruch,[1] V. Sharma,[2,3] C. dela Cruz,[4] R. Ramprasad,[2,3] and M. Jain[1,3]
[1]*Department of Physics, University of Connecticut, Storrs, Connecticut 06269, USA*
[2]*Materials Science and Engineering, University of Connecticut, Storrs, Connecticut 06269, USA*
[3]*Institute of Materials Science, University of Connecticut, Storrs, Connecticut 06269, USA*
[4]*Quantum Condensed Matter Division, Oak Ridge National Laboratory, Oak Ridge, Tennessee 37831, USA*

(Received 27 April 2014; accepted 8 July 2014; published online 18 July 2014)

The structure and magnetic ordering of bulk $TbMn_{0.5}Cr_{0.5}O_3$ was revealed through bulk magnetization and neutron diffraction measurements, and first-principles calculations, respectively. G-type antiferromagnetic ordering of Mn^{3+} and Cr^{3+} moments was observed in the neutron diffraction data below Néel temperature $T_N \sim 84$ K. In addition, below ~40 K, short-range magnetic ordering was identified correlating to a ferromagnetic component due to the canting of the moments along the *c*-axis. The spin configuration is consistent with the first-principles calculations. The magnetic structure revealed in the present $TbMn_{0.5}Cr_{0.5}O_3$ sample is distinct from that observed for both end members $TbMnO_3$ and $TbCrO_3$. © *2014 AIP Publishing LLC*. [http://dx.doi.org/10.1063/1.4890637]

INTRODUCTION

Single phase magnetoelectric (ME) multiferroics with coupling between ferroelectric and magnetic orders have been the focus of much research in the past decade due to their technological importance.[1,2] Large ME coupling is expected in perovskite rare-earth manganites ($RMnO_3$, R = Tb, Dy), as the development of ferroelectricity is inherently connected to the magnetic structure.[3–14] In particular, $TbMnO_3$ exhibits sinusoidal antiferromagnetic (AFM) ordering of Mn^{3+} moments at Néel temperature (T_N) ~ 41 K and noncollinear spiral spin (NSS) ordering of Mn^{3+} moments below ~28 K (referred to as T_{lock}).[3,5] Moreover, a ferroelectric polarization ordering develops below T_{lock} due to the inverse Dzyaloshinskii-Moriya exchange interaction[6,7] resulting in significant interdependence of magnetic and electric properties. However, this magnetoelectric effect in $TbMnO_3$ occurs at comparatively low temperatures and both magnetic moment and electric polarization are somewhat low to be considered for practical applications.

Chemical doping has been viewed as a useful way to tune the physical properties of materials with perovskite structure (ABO_3), as the structure offers a large degree of flexibility allowing various ionic substitutions at both cation sites.[15] Such notions have motivated previous studies of Sc, Co, or Fe substitution in the Mn site of $RMnO_3$ in the hope of increasing the transition temperature and inducing ferromagnetic (FM) interactions.[11–13] However, studies to-date have revealed that the low temperature multiferroic state is not robust—generally around 10% or 20% substitution of Mn (with either magnetic or non-magnetic ions) suppresses the NSS ordering and destroys ferroelectricity without considerably affecting T_{lock}.[11–14,16] It is therefore of great interest to critically examine the evolution of the multiferroic properties in B-site doped $RMnO_3$ with both end members as multiferroics.

Motivated by the above discussion, Cr is chosen as the B-site dopant in $TbMnO_3$ in the present work. $TbCrO_3$ exhibits G-type AFM ordering below $T_N \sim 157$ K with a FM component resulting in the canting of the moments along the *a*-axis (G_zF_x).[17,18] The ferroelectric behavior in $TbCrO_3$ was recently confirmed after the observation of reversible polar order below T_N by pyroelectric current measurements.[19] This polarization could be tuned by the application of a magnetic field, which would suggest a magnetically induced ferroelectric state that could also exhibit large ME coupling. Although the mechanism of ferroelectricity is not understood in the rare-earth chromites, the solid solution of $TbMnO_3$ and $TbCrO_3$ ($TbMn_{1-x}Cr_xO_3$) may be expected to retain multiferroic properties similar to one of the parent compounds throughout the solid solution.

Insight as to how the magnetic structure is modulated in this series is essential in understanding the evolution of the multiferroic properties. The present study therefore focuses on the determination of magnetic structure of $TbMn_{0.5}Cr_{0.5}O_3$ (TMCO) employing magnetization measurements, neutron diffraction, and first-principles calculations. In this material, a G-type AFM ordering is observed, but the Mn/Cr moments were aligned along the *a*-axis with a short range ferromagnetic spin correlation along the *c*-axis. A spin configuration unlike both parent compounds suggests that the present TMCO sample may exhibit unique multiferroic properties as well.

EXPERIMENTAL DETAILS

In order to make the bulk powder sample, high-purity precursors of Tb, Mn, and Cr were first mixed in solvent in stoichiometric ratio Tb(1)Mn(0.5)Cr(0.5). This solution was dried and the resultant powder was annealed at 900 °C for 2 h in oxygen to get the bulk TMCO powder. Temperature dependent dc magnetization data with 50 Oe (0.005 T) applied field were measured with a vibrating sample magnetometer attached to a Physical Property Measurement System (Quantum Design). Neutron powder diffraction was performed at the HB-2A beamline located at the High Flux

Isotope Reactor (Oak Ridge National Laboratory). The (113) reflection of a germanium wafer-stack monochromator was utilized resulting in a wavelength $\lambda = 2.4085$ Å. Neutron diffraction patterns were measured at temperatures between 3.4 K and 100 K. Rietveld refinement of the neutron diffraction data was performed with the FullProf suite.[20] Peaks from the sample holder were refined by profile matching with constant scale factor and the background was fitted by a linear interpolation between a set of background points with refinable height.

COMPUTATIONAL DETAILS

First-principles calculations using density functional theory (DFT) were performed using the projector-augmented wave method and a plane-wave cutoff energy of 500 eV, as implemented in the Vienna *ab initio* simulation package.[21–23] The exchange correlation interaction is treated within the generalized gradient approximation (GGA) using the Perdew-Burke-Ernzerhof functional.[24] It is worth mentioning that first principles results for the parent material $TbMnO_3$ (Ref. 25) are very sensitive to the choice of calculation parameters, especially the values of the on-site Coulomb energy (U). Therefore, in the present case, total energy calculations were also performed using the GGA plus the on-site repulsion (i.e., GGA + U) using a U value of 2.0 eV, which leads to exchange interactions between the Mn^{3+}/Cr^{3+} ions. The relaxation of atomic positions and optimization of lattice parameters were performed by the conjugate gradient method. All calculations were performed with and without including spin-orbital coupling (SOC). The atomic positions were relaxed until the maximum component of the force on each atom was smaller than 0.02 eV/Å. A Γ-centered k-point mesh of $3 \times 3 \times 2$ was employed to produce converged results within 0.1 meV per formula unit.

RESULTS

The temperature dependent zero-field cooled (ZFC) and field cooled (FC) dc magnetization data of the TMCO bulk powder are shown in Figure 1. Bifurcation of the ZFC and FC curves below ~84 K indicates the onset of ferromagnetic-like ordering. An anomaly in the ZFC data at 84 K, which can be observed clearly as a local minimum in the dM/dT plot, indicates the onset of long-range magnetic ordering. In addition, an anomaly in dM/dT plot at ~44 K suggests a second magnetic transition. It should be noted that the onset of magnetic ordering in the present TMCO sample is between that of the two end members of the solid solution ($T_N \sim 41$ K and ~157 K for $TbMnO_3$ and $TbCrO_3$, respectively), suggesting that the transition temperature in the $TbMnO_3$-$TbCrO_3$ solid solution is tunable by modifying the Mn/Cr ratio.

Rietveld refinement of the neutron powder diffraction pattern taken at 100 K suggests that TMCO is an orthorhombically distorted perovskite with the space group *Pbnm*. The resulting lattice parameters, M-O bond lengths and M-O-M bond angles ($M = Mn^{3+}$, Cr^{3+}), are presented in Table I. Results of the first-principles calculations performed with GGA and GGA + U (also reported in Table I) are close to the experimentally determined values, thus validating the use of these models for the TMCO system.

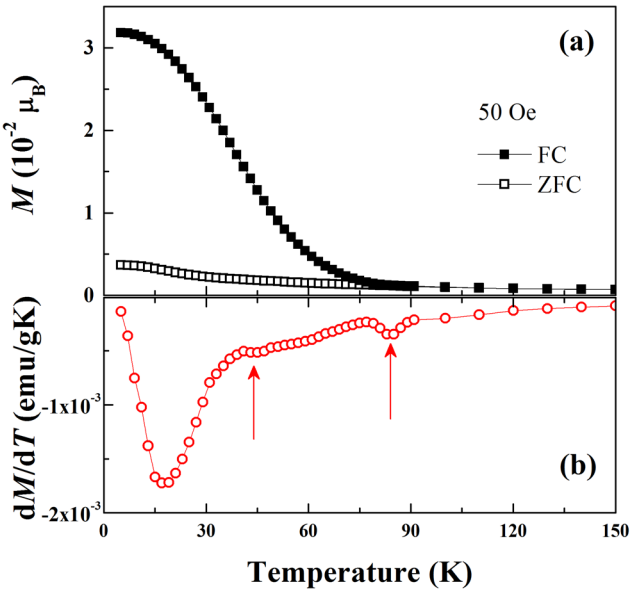

FIG. 1. (a) Temperature dependent zero-field cooled and field cooled magnetization of $TbMn_{0.5}Cr_{0.5}O_3$ with 50 Oe applied field. The kinks in the temperature dependent dM/dT data (b) indicate the onset of long range order of the Mn and Cr spins at T_N as well as a FM short range correlations at T_{SR}.

Figure 2(a) shows the refinement of the neutron powder diffraction pattern measured at 3.4 K. The appearance of intensity at $Q = 1.40$ Å^{-1} and 1.45 Å^{-1} upon cooling to 3.4 K indicates the onset of long range magnetic ordering. These peaks can be indexed to a magnetic propagation vector $k_m = (0, 0, 0)$. Refinement of the diffraction pattern taken at 3.4 K revealed that a G-type AFM alignment of both Mn^{3+} and Cr^{3+} moments with spins oriented along the a-axis best fits the data. The refinement of the nuclear and magnetic profile fits the data well with $R_p = 3.85$, $R_{wp} = 5.09$, and $\chi^2 \sim 4.89$. In modeling the low temperature magnetic phase, the Mn and Cr moments cannot be reliably refined independently. Therefore, the magnetic moment at each B-site was assumed to be equal and was found to saturate to (0.77 ± 0.05) μ_B per Mn/Cr site at 3.4 K. The intensity of the $(011)_M$ magnetic peak was tracked as a function of temperature and plotted as the corresponding static ordered moment at the B site {Figure 2(b)}. The transition temperature agrees with Néel temperature of ~84 K from bulk magnetization measurements. The precision in the moment along the b-axis and c-axis (determined as the value before a significant change in the reliability factor is observed) was ~0.01 μ_B, indicating that the spins lie almost completely along the a-axis.

Figure 3 displays the temperature evolution of the low-Q diffraction profile. There is a notable increase in intensity below 40 K in the form of a broad peak ~1.15 Å^{-1}. The broad, asymmetric Warren-type peak indicates the presence of short-range ordering in TMCO, which corresponds closely to the $(010)_M$ and $(100)_M$ reflections of the magnetic structure. Modeling of the data reveals that these peaks are consistent with a FM correlation along the c-axis in addition to the long range AFM order that sets in at T_N. This would

TABLE I. Summary of crystal structure parameters determined from Rietveld refinement results of the neutron powder diffraction pattern at 100 K, and 0 K DFT calculations using the GGA and GGA+U methods.

	Crystal structure of $TbMn_{0.5}Cr_{0.5}O_3$					
	Neutron powder diffraction			DFT GGA (GGA + *U*)		
a (Å)	5.301			5.309 (5.293)		
b (Å)	5.605			5.673 (5.697)		
c (Å)	7.505			7.595 (7.596)		
$d1_{Mn/Cr\text{-}O2}$ (Å)	2.059			2.023 (1.992)		
$d2_{Mn/Cr\text{-}O2}$ (Å)	1.956			1.944 (1.970)		
$d_{Mn/Cr\text{-}O1}$ (Å)	1.958			1.944 (1.970)		
Mn/Cr–O_2–Mn/Cr (deg)	147.7			147.4 (148.0)		
Mn/Cr–O_1–Mn/Cr (deg)	146.9			146.1 (146.6)		
Atomic coordinates:	*x*	*y*	*z*	*x*	*y*	*z*
Tb1 (4*c*)	0.983	0.070	0.250	0.981 (0.981)	0.073 (0.074)	0.250 (0.250)
O1 (4*c*)	0.100	0.469	0.250	0.109 (0.110)	0.464 (0.464)	0.249 (0.248)
O2 (8*d*)	0.700	0.308	0.049	0.693 (0.693)	0.302 (0.302)	0.056 (0.056)
Mn/Cr (4*b*)	0.500	0.000	0.000	0.500 (0.500)	0.000 (0.000)	0.000 (0.000)

suggest that the G-type AFM order is canted towards the *c*-axis at low temperatures. The short range FM correlation has an approximate in-plane correlation length of ~11.3 Å. The temperature dependence of the intensity at $Q_{SR} = 1.15$ Å^{-1} shows the onset of short-range magnetic order at $T_{SR} \sim 40$ K. These observations are consistent with dc magnetic data (Figure 1) as T_{SR} corresponds with the second peak observed in the d*M*/d*T* plot, suggesting that this anomaly develops as a result of a short range ferromagnetic correlation.

DFT calculations were performed to independently determine the possible low temperature magnetic ground state. In order to examine the most stable spin ordering in TMCO, energy optimization was performed with Mn^{3+} and Cr^{3+} ions alternating along *a* and *c* axes for possible spin configurations, such as FM, A-type AFM configuration, and G-type AFM ordering with spins oriented along the *a* as well as the *c*-axis, while assuming equivalent magnetic moment at each site, as shown in Figure 4. The results of the energy minimization calculations present consistency between the

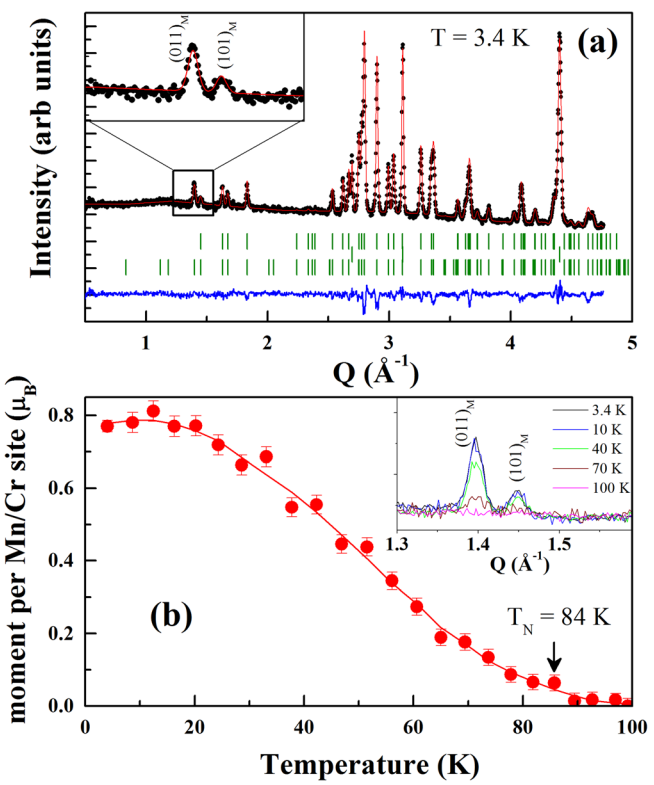

FIG. 2. (a) Rietveld refinement of the neutron powder diffraction data at 3.4 K with the structural model of TMCO, a phase representing the sample holder, and the magnetic phase. The magnetic phase is revealed to be a collinear G-type AFM ordering of the Mn and Cr spins along the *a*-axis. (b) Temperature dependence of the intensity of the $(011)_M$ magnetic reflection normalized to the saturated moment at 3.4 K of (0.77 ± 0.05) μ_B per Mn/Cr. The solid line is to guide the eye. The inset shows the $(011)_M$ and $(101)_M$ peaks at temperatures between 3.4 K and 100 K.

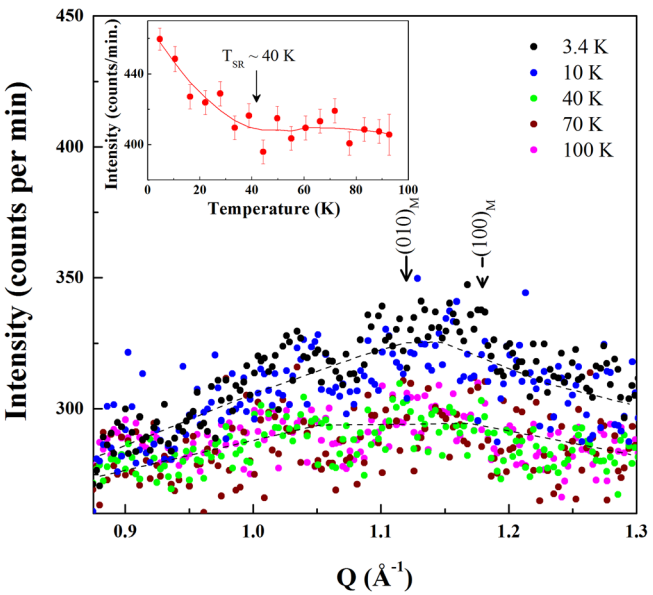

FIG. 3. Development of a broad peak at low Q with temperature around the positions of $(100)_M$ and $(010)_M$ indicating the presence of ferromagnetic correlations along the *c*-axis in addition to collinear in-plane AFM order of Mn^{3+} and Cr^{3+} spins. The inset shows the temperature dependence of the intensity of the short-range ordering peak centered at $Q = 1.15$ Å^{-1}, with an onset at $T_{SR} \sim 40$ K. Dashed/solid lines are guides for the eyes.

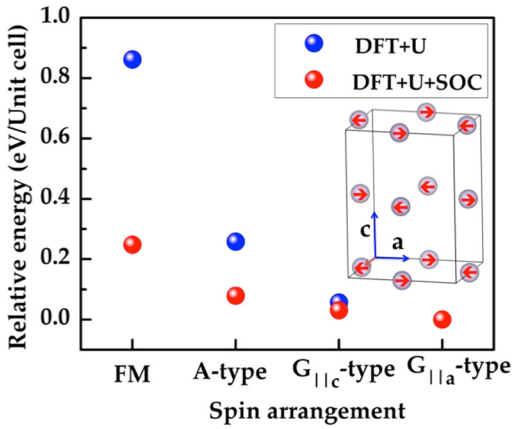

FIG. 4. DFT based energy optimization results for various spin arrangements in $TbMn_{0.5}Cr_{0.5}O_3$. The magnetic structure of Mn^{3+}/Cr^{3+} below T_N in the material as determined by neutron diffraction and DFT calculations is also shown in the inset. The structure shows equivalent moments at the B magnetic site that are ordered as a G-type antiferromagnet with spins along the *a*-axis. An additional short range ferromagnetic correlation develops below T_{SR} resulting in a canted spin-structure.

DFT + U and DFT + U + SOC results and reveal that a G-type collinear AFM spin structure imposed along the *a*-axis is the most stable magnetic configuration. This result is in agreement with the experimental data.

DISCUSSION

The complete spin configuration in TMCO at 3.4 K is revealed to be G-type AFM order with the Mn/Cr moments at the B-site ordered collinearly along the *a*-axis (as shown in Figure 4) with a FM component along the *c*-axis resulting in a canted orientation. This type of magnetic structure has been previously observed in proposed multiferroics $EuCrO_3$ and $YCrO_3$.[17,26] In $TbMnO_3$, utilizing neutron diffraction, the magnetic configuration was described with an incommensurate wave vector $k_M = (0, q, 0)$, where $q \sim 0.28$ below the ferroelectric transition temperature, T_{lock}.[5,27] No characteristic Bragg peaks associated with this ordering wave vector were detected in the present sample. The expected spin configuration for pure $TbCrO_3$ is G-type AFM with moments aligned along the *c*-axis and canted along *a*-axis.[17,18] This model is clearly not consistent with the data for present TMCO sample. Therefore, the possibility of phase coexistence with Mn-rich and Cr-rich regions is disregarded for the present TMCO sample and a *c*-axis canted collinear G-type AFM order along the *a*-axis is understood to be the global ordering of both Mn and Cr moments. These results are similar to previous neutron diffraction Mn/Cr substitution studies such as those in $LaMn_{1-x}Cr_xO_3$ or $NdMn_{1-x}Cr_xO_3$, where for $x \sim 0.5$, the coexistence of G-type AFM and FM structure was observed.[28,29]

Cation disorder at the B-site has been demonstrated to produce multiferroic behavior not found in the parent compounds.[30,31] Refinement with the space group *Pbnm* is consistent with disorder of Mn^{3+}/Cr^{3+} ions in the present TMCO sample that may result in this unique magnetic structure observed in both neutron diffraction data and first-principles calculations. Therefore, by adjusting the Mn/Cr ratio, not only can the transition temperature be tuned but also the spin configuration can be altered. The possibility that the multiferroic properties (such as the ferroelectric transition temperature or the direction of the electric polarization) can also be tuned in this manner will be investigated and presented separately in single crystal $TbMn_{0.5}Cr_{0.5}O_3$.

CONCLUSIONS

In summary, the structural and magnetic properties of bulk $TbMn_{0.5}Cr_{0.5}O_3$ were determined through bulk magnetization, neutron diffraction, and first-principles calculations. A G-type collinear antiferromagnetic spin configuration, with Mn^{3+} and Cr^{3+} moments oriented along the *a*-axis was observed below $T_N \sim 84$ K. This spin configuration was consistent with energy minimization from first-principles calculations. Short-range ferromagnetic ordering suggesting a canting of moments towards the *c*-axis is observed below $T_{SR} \sim 40$ K.

The present work leads to an important conclusion that the magnetic structure of $TbMn_{0.5}Cr_{0.5}O_3$ is distinct from that of both the end members, $TbMnO_3$ and $TbCrO_3$. It has been demonstrated that the transition temperature, spin configuration, and possibly the ferroelectric behavior of $TbMn_{1-x}Cr_xO_3$ can be tuned by controlling the Mn/Cr ratio. Thus, the engineering of novel multiferroics may be achieved through the modulation of magnetic interactions in well-known rare-earth manganite multiferroic materials through doping.

ACKNOWLEDGMENTS

The author M.J. is grateful for the financial support from National Science Foundation Grant DMR No. 1310149. The neutron diffraction measurements at the Oak Ridge National Laboratory's High Flux Isotope Reactor were sponsored by the Scientific User Facilities Division, Office of Basic Energy Sciences, U.S. Department of Energy. Computational support by an allocation from XSEDE is also gratefully acknowledged.

[1]M. Bibes and A. Barthélémy, Nature Mater. **7**, 425 (2008).
[2]Ch. Binek and B. Doudin, J. Phys.: Condens. Matter **17**, L39 (2005).
[3]T. Kimura, T. Goto, H. Shintani, K. Ishizaka, T. Arima, and Y. Tokura, Nature **426**, 55 (2003).
[4]T. Goto, T. Kimura, G. Lawes, A. P. Ramirez, and Y. Tokura, Phys. Rev. Lett. **92**, 257201 (2004).
[5]S. Quezel, F. Tcheou, J. Rossat-Mignod, G. Quezel, and E. Roudaut, Physica B+C **86–88**, 916(1977).
[6]A. Malashevich and D. Vanderbilt, Phys. Rev. Lett. **101**, 037210 (2008).
[7]C. Jia, S. Onoda, N. Nagaosa, and J. Han, Phys. Rev. B **74**, 224444 (2006).
[8]N. Zhang, Y. Y. Guo, L. Lin, S. Dong, Z. B. Yan, X. G. Li, and J.-M. Liu, Appl. Phys. Lett. **99**, 102509 (2011).
[9]M. Staruch, G. Lawes, A. Kumarasiri, L. F. Cotica, and M. Jain, Appl. Phys. Lett. **102**, 062908 (2013).
[10]N. Abe, K. Taniguchi, H. Sagayama, H. Umetsu, and T. Arima, Phys. Rev. B **83**, 060403 (2011).
[11]V. Cuartero, J. Blasco, J. García, J. Stankiewicz, G. Subías, J. A Rodriguez-Velamazán, and C. Ritter, J. Phys.: Condens. Matter **25**, 195601 (2013).
[12]V. Cuartero, J. Blasco, J. García, S. Lafuerza, G. Subías, J. A Rodriguez-Velamazán, and C. Ritter, J. Phys.: Condens. Matter **24**, 455601 (2012).
[13]F. Hong, Z. Cheng, H. Zhao, H. Kimura, and X. Wang, Appl. Phys. Lett. **99**, 092502 (2011).

[14]Y. Y. Guo, Y. J. Guo, N. Zhang, L. Lin, and J.-M. Liu, Appl. Phys. A **106**, 113 (2012).
[15]V. Sharma, G. Pilania, G. A. Rossetti, K. Slenes, and R. Ramprasad, Phys. Rev. B **87**, 134109 (2013).
[16]N. Zhang, K. F. Wang, S. J. Luo, T. Wei, X. W. Dong, S. Z. Li, J. G. Wan, and J.-M. Liu, Appl. Phys. Lett. **96**, 252902 (2010).
[17]E. Bertaut, J. Mareschal, G. de Vries, R. Aleonard, R. Pauthenet, J. Rebouillat, and V. Zarubicka, IEEE Trans. Magn. **2**, 453 (1966).
[18]J. D. Gordon, R. M. Hornreich, S. Shtrikman, and B. M. Wanklyn, Phys. Rev. B **13**, 3012 (1976).
[19]B. Rajeswaran, D. I. Khomskii, A. K. Zvezdin, C. N. R. Rao, and A. Sundaresan, Phys. Rev. B **86**, 214409 (2012).
[20]J. Rodríguez-Carvajal, Physica B: Condensed Matter **192**, 55 (1993).
[21]G. Kresse and J. Furthmüller, Comput. Mater. Sci. **6**, 15 (1996).
[22]G. Kresse, Phys. Rev. B **54**, 11169 (1996).
[23]G. Kresse and J. Hafner, Phys. Rev. B **49**, 14251 (1994).
[24]J. P. Perdew, K. Burke, and M. Ernzerhof, Phys. Rev. Lett. **77**, 3865 (1996).
[25]A. Malashevich and D. Vanderbilt, Phys. Rev. B **80**, 224407 (2009).
[26]V. Srinu Bhadram, B. Rajeswaran, A. Sundaresan, and C. Narayana, Europhys. Lett. **101**, 17008 (2013).
[27]M. Kenzelmann, A. Harris, S. Jonas, C. Broholm, J. Schefer, S. Kim, C. Zhang, S.-W. Cheong, O. Vajk, and J. Lynn, Phys. Rev. Lett. **95**, 087206 (2005).
[28]U. Bents, Phys. Rev. **106**, 225 (1957).
[29]I. O. Troyanchuk, M. V. Bushinsky, and D. V. Karpinsky, J. Exp. Theor. Phys. **103**, 580 (2006).
[30]P. Mandal, V. S. Bhadram, Y. Sundarayya, C. Narayana, A. Sundaresan, and C. N. R. Rao, Phys. Rev. Lett. **107**, 137202 (2011).
[31]B. Rajeswaran, P. Mandal, R. Saha, E. Suard, A. Sundaresan, and C. N. R. Rao, Chem. Mater. **24**, 3591 (2012).